New, improved bulk-microphysical schemes for studying precipitation processes in WRF.
Part I: Comparisons with other schemes

W.-K. Tao, J. Shi, S. S. Chen, S. Lang, S.-Y. Hong, G. Thompson, C. Peters-Lidard, A. Hou, and S. Braun, and J. Simpson

Submitted to Mon. Wea. Rev.

Popular Summary

Advances in computing power allow atmospheric prediction models to be run at progressively finer scales of resolution, using increasingly more sophisticated physical parameterizations and numerical methods. The representation of cloud microphysical processes is a key component of these models, over the past decade both research and operational numerical weather prediction models have started using more complex microphysical schemes that were originally developed for high-resolution cloud-resolving models (CRMs). A recent report to the United States Weather Research Program (USWRP) Science Steering Committee specifically calls for the replacement of implicit cumulus parameterization schemes with explicit bulk schemes in numerical weather prediction (NWP) as part of a community effort to improve quantitative precipitation forecasts (QPF).

An improved Goddard bulk microphysical parameterization is implemented into a state-of the-art of next generation of Weather Research and Forecasting (WRF) model. High-resolution model simulations are conducted to examine the impact of microphysical schemes on two different weather events (a midlatitude linear convective system and an Atlantic hurricane). The results suggest that microphysics has a major impact on the organization and precipitation processes associated with a summer midlatitude convective line system. The 3ICE scheme with a cloud ice-snow-hail configuration led to a better agreement with observation in terms of simulated narrow convective line and rainfall intensity. This is because the 3ICE-hail scheme includes dense ice precipitating (hail) particle with very fast fall speed (over 10 m s^{-1}). For an Atlantic hurricane case, varying the microphysical schemes had no significant impact on the track forecast but did affect the intensity (important for air-sea interaction).

New, improved bulk-microphysical schemes for studying precipitation processes in WRF.
Part I: Comparisons with other schemes

W.-K. Tao[1], J. Shi[1,2], S. S. Chen[3], S. Lang[1,4], S.-Y. Hong[5], G. Thompson[6], C. Peters-Lidard[7], A. Hou[8], and S. Braun[1], and J. Simpson[1]

[1]*Laboratory for Atmospheres*
NASA Goddard Space Flight Center
Greenbelt, Maryland

[2]*Science Applications International Corporation*
Beltsville, Maryland

[3]*Rosentiel School of Marine and Atmospheric Science*
University of Miami
Miami, Florida

[4]*Science Systems and Applications, Inc.*
Lanham, Maryland

[5]*Global Environment Laboratory, Department of Atmospheric Sciences*
Yonsei University
Seoul, South Korea

[6]*National Center for Atmospheric Research (NCAR)*
Boulder, Colorado

[7]*Hydrological Sciences Branch*
NASA Goddard Space Flight Center
Greenbelt, Maryland

[8]*Goddard Modeling Assimilation Office*
Greenbelt, MD 20771

May 24, 2007

Mon. Wea. Rev.

---

[1] *Corresponding author address: Dr. Wei-Kuo Tao, Code 613.1, NASA Goddard Space Flight Center, Greenbelt, MD 20771, tao@agnes.gsfc.nasa.gov*

Abstract

An improved bulk microphysical parameterization is implemented into the Weather Research and Forecasting (WRF) model. This bulk microphysical scheme has three different options, 2ICE (cloud ice & snow), 3ICE-graupel (cloud ice, snow & graupel) and 3ICE-hail (cloud ice, snow & hail). High-resolution model simulations are conducted to examine the impact of microphysical schemes on two different weather events (a midlatitude linear convective system and an Atlantic hurricane). In addition, the improved schemes are compared with WRF's three other bulk microphysical schemes.

The results suggest that microphysics has a major impact on the organization and precipitation processes associated with a summer midlatitude convective line system. The 3ICE scheme with a cloud ice-snow-hail configuration led to a better agreement with observation in terms of simulated narrow convective line and rainfall intensity. This is because the 3ICE-hail scheme includes dense ice precipitating (hail) particle with very fast fall speed (over 10 m s^{-1}). For an Atlantic hurricane case, varying the microphysical schemes had no significant impact on the track forecast but did affect the intensity (important for air-sea interaction).

The vertical distributions of model simulated cloud species (i.e., snow) are quite sensitive to microphysical schemes, which is an important issue for future verification against satellite retrievals. Sensitivity tests are performed to identify that snow productions could be increased by increasing the snow intercept, turning off the auto-conversion from snow to graupel and reducing the transfer processes from cloud-sized particles to precipitation-sized ice.

1. Introduction

Advances in computing power allow atmospheric prediction models to be run at progressively finer scales of resolution, using increasingly more sophisticated physical parameterizations and numerical methods. The representation of cloud microphysical processes is a key component of these models, over the past decade both research and operational numerical weather prediction models [i.e., the Fifth-generation National Center for Atmospheric Research (NCAR)/Penn State University Mesoscale Model (MM5), the National Centers for Environmental Prediction (NCEP) Eta, and the Weather Research and Forecasting Model (WRF)] have started using more complex microphysical schemes that were originally developed for high-resolution cloud-resolving models (CRMs). CRMs, which are run at horizontal resolutions on the order of 1-2 km or finer, can simulate explicitly complex dynamical and microphysical processes associated with deep, precipitating atmospheric convection. Chen *et al* (2007) showed the importance of high-resolution in the fully coupled air-sea models for hurricane prediction. A recent report to the United States Weather Research Program (USWRP) Science Steering Committee specifically calls for the replacement of implicit cumulus parameterization schemes with explicit bulk schemes in numerical weather prediction (NWP) as part of a community effort to improve quantitative precipitation forecasts (QPF, Fritsch and Carbone 2002).

There is little doubt that cloud microphysics play an important role in non-hydrostatic high-resolution simulations. For example, microphysics and their effect on precipitation processes, hurricanes and other severe weather events have been studied extensively over the

past two decades (i.e., Yoshizaki 1986; Nicholls 1987; Fovell and Ogura 1988; Tao and Simpson 1989; Zhang 1989; McCumber *et al.* 1991; Ferrier *et al.* 1995; Tao *et al.* 1995; Krueger *et al.* 1995; Fu *et al.* 1995; Liu *et al.* 1997; Wu *et al.* 1999; Thompson *et al.* 2004; Colle *et al.* 2004; Zhu and Zhang 2004; and many others). Generally, two different approaches were used to examine the impact of microphysics on precipitation processes associated with convective systems. The first approach is to examine the sensitivity of different microphysical schemes on precipitation processes (i.e., McCumber *et al.* 1991; Ferrier *et al.* 1995; Tao *et al. 2003a, b;* and others). This approach can help to identify the strength(s) and/or weakness(es) of each scheme in an effort to improve their performance. The second approach is to examine specific microphysical processes (i.e., melting, evaporation) within one microphysical scheme. This approach can identify the dominant microphysical process(es) in determining the organization and structure of convective systems. This paper will apply the first approach and examine the performance of different microphysical schemes.

An improved bulk microphysics parameterization (Tao *et al.* 2003a; Lang *et al.* 2007) has recently been implemented into the high-resolution non-hydrostatic WRF. The major objective of this paper is to test the performance of the revised microphysics in WRF. Numerical experiments will be performed for two different weather events, a midlatitude linear convective system and an Atlantic hurricane, to investigate the impact of the microphysical parameterization on organization, evolution/propagation, intensity, and vertical distribution of cloud species, and rainfall intensity. A more detailed comparison

study using observational data to evaluate/validate the cloud microphysical schemes will be presented in Part II (Shi *et al.* 2007).

2. Description of microphysical schemes

2.1 Goddard microphysical schemes

The Goddard Cumulus Ensemble (GCE) model's (Tao and Simpson 1993) one-moment bulk microphysical schemes were recently implemented into WRF. These schemes are mainly based on Lin *et al.* (1983) with additional processes from Rutledge and Hobbs (1984). However, the Goddard microphysics schemes have several modifications. First, there is an option to choose either graupel or hail as the third class of ice (McCumber *et al.* 1991). Graupel has a relatively low density and a high intercept value (i.e., more numerous small particles). In contrast, hail has a relative high density and a low intercept value (i.e., more numerous large particles). These differences can affect not only the description of the hydrometeor population and formation of the anvil-stratiform region but also the relative importance of the microphysical-dynamical-radiative processes. Second, a new saturation technique (Tao *et al.* 1989) was added. This saturation technique is basically designed to ensure that super saturation (sub-saturation) cannot exist at a grid point that is clear (cloudy). The saturation scheme is one of the last microphysical processes to be computed. It is only done prior to evaluating evaporation of rain and snow/graupel/hail deposition or sublimation. Third, all microphysical processes that do not involve melting, evaporation or sublimation (i.e., transfer rates from one type of hydrometeor to another) are calculated based on one

thermodynamic state. This ensures that all of these processes are treated equally. The opposite approach is to have one particular process calculated first modifying the temperature and water vapor content (i.e., through latent heat release) before the next process is computed. Fourth, the sum of all sink processes associated with one species will not exceed its mass. This ensures that the water budget will be balanced in the microphysical calculations[1].

In addition to the two different 3ICE schemes (i.e., cloud ice, snow and graupel or cloud ice, snow and hail) implemented into WRF, the Goddard microphysics has a third option, which is equivalent to a two-ice (2ICE) scheme having only cloud ice and snow. This option may be needed for coarse resolution simulations (i.e., > 5 km grid size). The two-class ice scheme could be applied for winter and frontal convection.

Recently, the Goddard 3ICE schemes were modified to reduce over-estimated and unrealistic amounts of graupel in the stratiform region (Tao *et al.* 2003a; Lang *et al.* 2007). Various assumptions associated with the saturation technique were also revisited and examined (Tao *et al.* 2003a). These modifications are described below.

(a) Saturation adjustment

When supersaturated conditions are brought about, condensation or deposition is required to remove any surplus of water vapor. Likewise, evaporation or sublimation is required to

---

1 The above Goddard microphysical scheme has been implemented into the MM5 and ARPS.

balance any vapor deficit when sub-saturated conditions are made to occur in the presence of cloud. As the saturation vapor pressure is a function of temperature, and the latent heat released due to condensation, evaporation, deposition, and sublimation modifies the temperature, one approach has been to solve for the saturation adjustment iteratively. Soong and Ogura (1973), however, put forth a method that did not require iteration but for the water-phase only.

Tao *et al.* (1989) adopted the approach of Soong and Ogura (1973) and modified it to include the ice-phase. For temperatures over T_0 (0 ^oC), the saturation vapor mixing ratio is the saturation value over liquid water. For temperatures below T_{00}, which typically ranges from -30 to -40 ^oC, the saturation vapor mixing ratio is the saturation value over ice. The saturation water vapor mixing ratio between the temperature range of T_0 and T_{00} is taken to be a mass-weighted combination of water and ice saturation values depending on the amounts of cloud water and cloud ice present. Condensation/deposition or evaporation/sublimation then occurs in proportion to the temperature. Another approach is based on a method put forth by Lord *et al.* (1984), which weights the saturation vapor mixing ratio according to temperature between 0C and T00. Condensation/deposition or evaporation/sublimation is then still proportional to temperature. One other non-iterative technique treats condensation and deposition or evaporation and sublimation sequentially. Saturation adjustment with respect to water is allowed first for a specified range of temperatures followed by an adjustment with respect to ice over a specified range of temperatures. The temperature is allowed to change after the water phase before the ice

phase is treated. Please refer to Tao *et al.* (2003a) for the performance of these three different adjustment schemes. All three approaches are available with WRF.

These adjustment schemes will almost guarantee that the cloudy region (defined as the area which contains cloud water and/or cloud ice) is always saturated (100% relative humidity). This permits sub-saturated downdrafts with rain and hail/graupel particles but not cloud-sized particles.

(b) Conversion of cloud particles to precipitation-sized ice

Lang *et al.* (2007) have simulated two types of convective cloud systems that formed in two distinctly different environments observed during the Tropical Rainfall Measuring Mission Large-Scale Biosphere–Atmosphere (TRMM LBA) experiment in Brazil. Model results showed that eliminating the dry growth of graupel in the Goddard 3ICE bulk microphysics scheme effectively removed the unrealistic presence of high-density ice in the simulated anvil. However, comparisons with radar reflectivity data using contoured-frequency-with-altitude diagrams (CFADs, see Yuter and Houze 1995) revealed that the resulting snow contents were too large. The excessive snow was reduced primarily by lowering the collection efficiency of cloud water by snow and resulted in further agreement with the radar observations. The transfer of cloud-sized particles to precipitation-sized ice appears to be too efficient in the original scheme. Overall, these changes to the microphysics lead to more realistic precipitation ice contents in the model. The improved precipitation-sized ice signature in the model simulations lead to better latent heating retrievals as a result of both

better convective-stratiform separation within the model as well as more physically realistic hydrometeor structures for radiance calculations. However, there appeared to be additional room for improvement in that simulated brightness temperatures showed that there was still too much precipitation-sized ice aloft. This indicates that despite the improvement, the overall transfer rate of cloud-sized particles to precipitation-sized particles was still too efficient. Lang *et al.* (2007) felt that the Bergeron process could be a contributing factor.

(c) The Bergeron process

An important process in the budget for cloud ice is the conversion of cloud ice to snow as the ice crystals grow by vapor deposition in the presence of cloud water, usually referred to as the Bergeron process and designated P_{SFI} (production of snow from ice) by Lin *et al.* (1983). The formulation generally used in the parameterization is independent of relative humidity, which causes ice to be converted to snow even when the air is subsaturated with respect to ice. One alternative formulation is to simply multiply the original formula by a relative-humidity dependent factor so that P_{SFI} diminishes as the relative humidity approaches the ice saturation value. A second alternative formulation can be derived directly from the equation for depositional growth of cloud ice (Rutledge and Hobbs 1984) used in the model. This formulation also causes PSFI to diminish as the relative humidity approaches the ice saturation value and is physically consistent with the parameterization for depositional growth of cloud ice. The two alternative formulations produce relatively similar results since simulated ice clouds over tropical oceans often have vapor mixing ratios near the ice saturation value so that PSFI is very small. The new formulation for P_{SFI} based on

the simple relative-humidity correction factor was adopted and results in an increase in cloud-top height and a substantial increase in the cloud ice mixing ratios, particularly at upper levels in the cloud.

2.2 *Microphysical schemes in WRF*

Currently, WRF has three different one-moment bulk microphysical parameterizations involving the same classes of five hydrometeors (cloud water, rain, cloud ice, snow, and graupel). All parameterized production terms in all schemes except Thompson *et al.* (2004, 2007) are basically based on Lin *et al.* (1983) and Rutledge and Hobbs (1984) with relatively minor modifications. Differences between GCE and LFO were discussed in the previous subsection. The most dominant changes for the WSM6 and Thompson schemes are briefly mentioned below.

The WRF-Single-Moment 6-Class Microphysics (WSM6) scheme (Hong and Lim 2006) also has five classes of hydrometeors as in the Purdue Lin scheme, but with the revised ice microphysics proposed by Hong *et al.* (2004). The most distinguishing features of the Hong *et al.* (2004) are that (1) it practically represents ice microphysical processes by assuming the ice nuclei number concentration to be a function of temperature and (2) it involves the new assumption that the ice crystal number concentrations are a function of the amount of ice. The related ice processes are changed accordingly. The saturation adjustments are based on Tao *et al.* (2003a) and separately treat the ice and water saturation processes. Hong *et al.* (2004) showed that significant improvements were made in high

cloud amount, surface precipitation, and large-scale mean temperature through better representation of the ice-radiation feedback. A detailed description of the WSM6 scheme including all the source/sink terms and the computational procedures are given in Hong and Lim (2006).

The Thompson *et al.* (2007) scheme was designed to improve the prediction of freezing drizzle events for aircraft safety. Like the other schemes, this scheme has the same five classes of hydrometeors plus a prognostic ice number concentration. Whereas the previous version of WRF (v2.1) used the Thompson *et al.* (2004) code, which was primarily based on Reisner *et al.* (1998), this research utilized an entirely new Thompson *et al.* (2007) scheme found in WRF v2.2 that dramatically differs from the LFO-based schemes. Most importantly, none of the intercept parameters is constant and all species assume a generalized gamma distribution instead of the purely exponential distribution. The intercept parameter for rain is diagnosed from rain mixing ratio and/or from equivalent melted snow/graupel diameter relationships. The snow intercept parameter depends on both temperature and snow water content to match observations by Field *et al.* (2005). The graupel intercept parameter depends on its mixing ratio and, as such, allows the graupel category to mimic both graupel and hail. In conditions of light to moderate updrafts, smaller particle graupel (mostly from rimed snow) dominates with a terminal velocity relation more similar to snow than hail. However, in relatively strong updrafts, the intercept parameter significantly decreases and the resulting terminal velocity is similar to observations for hail. Additional improvements, such as the treatment of autoconversion and hydrometeor collision/collection, can be found in Thompson *et al.* (2007).

2.3 Water Budget Adjustment

A 3rd order finite difference method is used in WRF (Wicker and Skamarock 2002). It is well known that this difference method can generate negative mass for hydrometeors near and at cloud boundaries. The adjustment used in WRF is to reassign all negative hydrometeors to be zero. This can cause an imbalance in the water budget. Note that the error grows with the number of time iterations not the length of model integration.

To remedy this shortcoming (especially for long term model integration and for fine resolution simulations), a mass conservation-adjustment scheme was implemented into WRF. The procedure for this mass conservation scheme for all hydrometeors is as follows: (1) compute the total positive mass (P) and negative mass (N) over the entire domain, (2) set all negative mass to be zero, and (3) re-compute the positive mass by multiplying by a factor of (P-N)/P. This type of adjustment has been used in many cloud-scale models (i.e., Soong and Ogura 1973; the GCE model, and many others).

3. Model set-up and cases

To examine the generality and applicability of the microphysical schemes, two different types of precipitation systems, a midlatitude convective system and an Atlantic hurricane (Fig. 1), were selected to test the performance of the Goddard microphysical scheme with its different options (i.e., 2ICE and both 3ICE versions). For comparison, simulations for the

same case studies using WRF and the other three microphysical schemes (i.e., Purdue Lin, WSM6 and Thompson) are also presented.

3.1 A midlatitude mesoscale convective system case

The International H2O project (IHOP_2002) was conducted over southern Kansas, Oklahoma, and northern Texas for six weeks during May and June of 2002 (13 May to 25 June 2002). Its focus was to obtain atmospheric water vapor profiles and relate them to convection initiation (CI), atmospheric boundary layer development (ABL) and quantitative precipitation forecasting (QPF). The case selected is a linear convective system (see Fig. 1) that occurred between 1200 UTC 12 and 1200 UTC 13 June. The event fell on a major IHOP study day with there being a small-scale low-pressure center located in the Oklahoma Panhandle before the development of the convective bands. Scattered strong storms started growing by 2100 UTC 12 June and then organized into a strong squall line by 0000 UTC 13 June. At that time, there were two major rain bands oriented from northeast to southwest, which stretched from southeast Kansas through the eastern part of the Oklahoma Panhandle and into the Texas Panhandle. By 0300 UTC 13 June, the linear convective system had advanced into central Oklahoma and was continuing to move southeast. Although the line had been quite strong with a substantial trailing stratiform area, it dissipated quickly after 0900 UTC and was gone by 1200 UTC as it moved into Arkansas. Despite the system's short life span, maximum accumulated rainfall reached 100 mm at some locations over the 18-hour time period.

Multiple nested domains were constructed with grid resolutions of 9, 3 and 1 km, respectively; the corresponding numbers of grid points are 301 x 202 x 31, 481 x 352 x 31, and 541 x 466 x 31 (Fig. 2). Time steps of 30, 10 and 3.333 seconds were used in these nested grids, respectively. The largest domain covers almost the entire US. The finest domain covers the entire IHOP region and the immediate vicinity. The model was initialized from NOAA/NCEP global analyses (2.5^{o} by 2.5^{o}). Time-varying lateral boundary conditions were provided at 6-h intervals. The model was integrated from 00 UTC 12 June to 12 UTC 13 June 2002.

The Kain-Fritsch (1990, 1993) cumulus parameterization scheme was used for the coarse 9 km grid mesh. In the 3 and 1 km grid domain, the Kain-Fritsch parameterization scheme was turned off. The WRF atmospheric radiation model includes longwave and shortwave parameterizations that interact with the atmosphere. The shortwave scheme uses a broadband two-stream (upward and downward fluxes) approach for the radiative flux calculations (Dudhia 1989). The longwave scheme is based on Mlawer *et al.* (1997) and is a spectral-band scheme using the correlated-k method. The planetary boundary layer parameterization employed the Mellor-Yamada-Janjic (Mellor and Yamada 1992, and coded/modified by Dr. Janjic for NCEP Eta model) Level 2 turbulence closure model through the full range of atmospheric turbulent regimes. The surface heat and moisture fluxes (from both ocean and land) were computed from similarity theory (Monin and Obukhov 1954). The land surface model is based on Chen and Dudhia (2001). It is a 4-layer soil temperature and moisture model with canopy moisture and snow cover prediction. It provides sensible and latent heat fluxes to the boundary layer scheme.

3.2 An Atlantic hurricane case

In addition to the midlatitude MCS, a hurricane case, Katrina 2005, was examined using WRF with different microphysical schemes. Katrina was among the most significant, intense, and dangerous storms to occur in the Gulf of Mexico in the history of the United States. It is the sixth most intense Atlantic hurricane on record (fourth at the time of occurrence) with a minimum observed central pressure of 902 hPa (Houze *et al.* 2006), the third most intense hurricane to make landfall in the US, the costliest with an estimated damage total of over $80 billion US, and the deadliest since 1928 with at least 1836 fatalities. The twelfth tropical depression (TD#12) of the 2005 Atlantic hurricane season formed on the afternoon (local time) of 23 August 2005 in the southeastern Bahamas when a propagating easterly wave interacted with the remnants of TD#10. The system was upgraded to a tropical storm on the morning of the 24th and given the name Katrina when it was in the central Bahamas. After turning west out of the Bahamas, it strengthened into a minimal Category 1 hurricane after passing over the Gulf Stream before quickly making landfall in southwest Florida south of Fort Lauderdale on the morning of the 24th. Katrina weakened only slightly as it quickly made its way across the wet marshes of the Florida Everglades. Katrina re-emerged over open water early on the morning of the 26th into the southeastern Gulf of Mexico moving west-southwest and quickly regained hurricane intensity. By mid-morning Katrina was a category 2 storm and remained at that level through the early evening. Atmospheric conditions were favorable for strengthening as Katrina moved over the Loop Current, a deep warm eddy of the Gulf Stream that extends from the southeastern into the

central Gulf of Mexico. These conditions allowed Katrina to strengthen into a strong category 3 storm on the 27th. Figure 1b shows Katrina in the central Gulf as seen by the Tropical Rainfall Measuring Mission (TRMM) satellite. The images were taken at 03:24 UTC 28 August 2005 (10:24 pm CDT 27 August 2005). TRMM reveals that Katrina is a large symmetrical storm with a well-defined eye surrounded by tightly-curving rain bands—all characteristic of a mature, intense tropical cyclone. A deep area of convection is also evident in the eyewall, which can often indicate intensification. During the night of the 27th, Katrina began a rapid deepening cycle, which brought the storm to category 5 intensity on the morning of the 28th. By now, Katrina was moving more northward through a weakness in the subtropical ridge ahead of an advancing trough from the west, taking it on a course for the central northern Gulf Coast. Maximum sustained winds dropped as the massive storm approached southeast Louisiana due to another eyewall replacement cycle, and Katrina made landfall on the morning of the 29th as a strong category 3 storm.

Three multiple nested domains (Fig. 3) were constructed with grid resolutions of 15, 5 and 1.667 km, respectively; the corresponding numbers of grid points are 300 x 200 x 31, 418 x 427 x 31, and 373 x 382 x 31. The innermost domain moves with the center of the storm. The model was integrated for 72 h from 00 UTC 27 August to 00 UTC 30 August 2005. A large inner domain was necessary for the Hurricane Katrina simulations because it was both an intense Category 5 hurricane and a large storm. A moving nested domain was also necessary because Hurricane Katrina moved quickly. Time steps of 30, 10 and 3.333 seconds were used in the nested grids, respectively. The model was initialized from NOAA/NCEP/GFS global analyses (2.5° by 2.5°). Time-varying lateral boundary

conditions were provided at 6-h intervals.

The Grell-Devenyi (2002) cumulus parameterization scheme was used for the outer grid (15 km) only. For the inner two domains (5 and 1.667 km), the Grell-Devenyi parameterization scheme was turned off. The Goddard broadband two-stream (upward and downward fluxes) approach was used for the shortwave radiative flux calculations (Chou and Suarez 1999). The longwave scheme was the same used for the MCS simulations based on Mlawer *et al.* (1997). Likewise, the planetary boundary layer parameterization and the surface heat and moisture fluxes (from both ocean and land) follow the MCS case.

4. Results

4.1 *The 12 June IHOP Case*

Figure 4 shows the WRF-simulated radar reflectivity from six different microphysical schemes. Generally speaking, WRF produced the right distribution of precipitation for this IHOP case despite using different microphysical schemes. For example, in all of the runs the major precipitation event is elongated in the southwest-northeast direction. WSM6 and Purdue Lin are similar, but the local maximum is smaller in WSM6 due to the smaller fall velocities of graupel and a different radiation feedback in the revised ice-microphysics in WSM6 (Hong *et al.* 2007). The Thompson scheme produced a broader area of light precipitation than WSM6 and Purdue Lin. The Goddard 3ICE-hail scheme resulted in a very thin convective line in the Texas Panhandle and northern Oklahoma, which agrees best with

observations (Fig. 1). As would be expected, the simulated linear convective system is broader and less intense when using the Goddard 2ICE or 3ICE-graupel schemes. This is because snow and graupel have lower densities and hence slower fall speeds than hail. Snow or graupel forming in the convective cores can ascend to higher altitudes than hail and then be carried farther downstream from the convection before descending through the melting region. Consequently, surface rain is spread over a wider area. Snow has a slower fall speed than graupel; therefore, surface rain occurs over an even larger area with the 2ICE physics as compared to 3ICE-graupel. The Purdue Lin scheme also simulated a thin convective line.

Both the vertical distribution of cloud species and the surface rainfall PDF are sensitive to the microphysical schemes. Figure 5 shows PDFs of the WRF-simulated and observed surface rainfall intensity. The 2ICE scheme produced more light rain (less than 8 mm/h) and less total rainfall than the others. This is because the snow particles remain longer in the middle and upper troposphere and do not fall as rapidly through the melting layer. This implies that the precipitation efficiency is lower for the 2ICE scheme. The Goddard 3ICE-graupel scheme generally produced lighter and less intense precipitation compared to the 3ICE-hail scheme. Both the 3ICE-hail and Thompson schemes resulted in less light precipitation (8 mm/h or less) and more moderate rainfall (> 16 mm/h and < 48 mm/h). These results seem to be in better agreement with observations. However, the 3ICE-hail and Thompson schemes also simulated too much heavy rainfall (i.e., > 48 mm/h) compared to the observations and other schemes. The results from the WSM6 scheme are quite similar to the 2ICE scheme. The Purdue Lin scheme agrees better with the observations than does WSM6. The rainfall intensity (heavy or light rainfall) can be very

important for surface processes (e.g., hydrological as well as ocean mixed layer models).

Figure 6 shows vertical profiles of the domain- and time-averaged cloud species (i.e., cloud water, rain, cloud ice, snow and graupel or hail). The Purdue Lin and WSM6 microphysical schemes simulated much less snow compared to the other four schemes. The Thompson scheme simulated very little cloud ice. Its simulated snow peak is above 300 hPa, which is higher than other schemes, and its simulated graupel profile extends below the melting layer. The Goddard 2ICE and 3ICE-graupel schemes both produced more cloud ice than did the 3ICE-hail scheme (similar results were also obtained in earlier GCE model simulations, see McCumber *et al.* 1991). The Thompson and Goddard 3ICE-graupel schemes produced large snow profile. This is because the Thompson and Goddard 3ICE-graupel schemes both assume a similar snow intercept parameter (0.20 and 0.16, respectively). The snow intercept is one order of magnitude smaller in Purdue Lin (0.02). This could explain the smaller amount of snow in Purdue Lin scheme. The snow intercept parameter in WSM6, however, is a function of T and it varies from 0.02 (0 C) to 2.43 (-40 C). The Purdue Lin, WSM6 and Goddard 3ICE schemes are all basically based on Lin *et al.* (1983) and Rutledge and Hobbs (1984). The new modifications to the Goddard schemes described in section 2 might also increase snow production in the Purdue Lin and WSM6 schemes. Additional sensitivity tests on enhanced snow production in Purdue Lin and WSM6 are described in section 4.3. An accurate vertical distribution of cloud species (snow in particular) is important for satellite rainfall retrieval (Lang *et al.* 2007).

Table 1 gives the relative fraction of liquid (cloud water and rain) and solid (cloud

ice, snow and graupel or hail) water contents based on time-domain averages for each scheme. The Goddard 3ICE-hail and WSM6 microphysical schemes both resulted in similar liquid (~40%) and solid (~60%) fractions. The Goddard 3ICE-graupel and Thompson schemes produced higher ice fractions than 3ICE-hail and WSM6. The Goddard 2ICE scheme produced very little liquid while the Purdue Lin scheme produced more warm rain (liquid phase) than the other schemes.

4.2 Hurricane Katrina

Figures 7a and 7b show the simulated minimum sea level pressure (MSLP) and track, respectively, from WRF using six different microphysical schemes: Goddard 2ICE, 3ICE-hail, 3ICE-graupel, Purdue Lin, WSM6 and Thompson. The simulated hurricane is stronger than was observed (i.e., the 48-hour simulated MSLP was too low) in all cases. However, this over-estimate in the intensity forecast after the first 24 hours may have resulted from inaccurate SSTs in the global analysis and weaker vertical wind shear and cold air intrusion from the west (see the detailed discussions in Part II). Simulated MSLP using the 2ICE and Thompson schemes are the closest to the observations (from 24 to 48 hours into the forecast). Note that both (2ICE and Thompson) schemes simulated less (or no) graupel compared to the other schemes (Fig. 8). Minimum sea surface pressures from the Goddard 3ICE and WSM6 schemes are quite similar to each other. The Purdue Lin scheme, however, results in a minimum sea surface pressure 15-20 hPa lower than the other schemes. Nevertheless, the simulated temporal variation of MSLP agrees well with observations (i.e., intensification prior to landfall followed by weakening). Further analysis will be conducted to diagnose the

mechanism (s) responsible for the different storm intensity, especially the dynamic fields (i.e., vertical velocity) as shown in Rogers *et al.* (2007). The sensitivity tests show no significant difference (or sensitivity) in track among the different microphysical schemes. The simulated tracks are very similar prior to landfall (the first 48 hours of model integration time). After landfall, the simulated tracks remain closely packed with the storm center propagating to the north-northeast. All the simulations result in landfall farther west than was observed. The exaggerated storm intensities in the model may have caused the bias in storm track.

Figure 8 shows vertical profiles of the domain- and time-averaged cloud species for Hurricane Katrina. The main differences between the Goddard, Thompson, Purdue Lin and WSM6 microphysical schemes are in the solid phase of water species at middle and upper levels. Graupel is the dominant ice species in Purdue Lin and WSM6, while very little cloud ice is simulated by the Thompson scheme. These were also apparent in the IHOP case. Purdue Lin and WSM6 produce very little snow (similar results were also found for another hurricane simulated by WRF) but more warm rain than the other schemes (see Table 2). The Thompson scheme has a solid ice fraction similar to the Goddard 3ICE-graupel scheme but with a broader snow distribution, and the Goddard 2ICE scheme has the least warm rain of all the schemes. Similar results were also found in the IHOP case. Additional analysis of the model results (i.e., convective vs stratiform, CFADs) is available in Part II.

4.3 Modification of Purdue Lin and WSM6

The Purdue Lin and WSM6 microphysical schemes simulated very little snow compared to the Goddard and Thompson microphysical schemes for both the IHOP and Hurricane Katrina cases. There are two possible reasons for the difference in snow. One is the different intercept parameter used in the Purdue Lin and WSM6 schemes. Another is the conversion process between cloud species. Four additional sensitivity tests were conducted using the Purdue Lin and WSM6 microphysical schemes. In the first two tests, the snow intercepts were modified from their original value to 0.16 (the value in the Goddard scheme and without the temperature dependency of WSM6) and the auto-conversion from snow to graupel was turned off along with a reduction in the transfer processes from cloud-sized particles to precipitation-sized ice (Lang *et al.* 2007) for Purdue Lin and WSM6 schemes. In the third and fourth tests, the snow intercepts were kept at the original values for Purdue Lin and WSM6. The sensitivity tests were performed for the IHOP case.

Figure 9 shows vertical profiles of the domain- and time-averaged ice species (cloud ice, snow and graupel) from the sensitivity tests using the Purdue-Lin and WSM6 microphysical schemes with modifications. These modifications (increasing snow intercept parameter and tuning off some of transfer processes related to snow production/reduction) do have an impact on snow production as evidenced by the increased snow amounts for both the Purdue-Lin and WSM6 schemes. For the Purdue-Lin scheme, the amount of snow increased significantly; for the WSM6 scheme, however, the increase in snow was much more modest without increasing the snow intercept parameter. The change of the snow intercept parameter can enhance snow

production in both WSM6 and Purdue scheme (compare the snow profiles shown in Figs. 9(a) and 9(b), and 9(c) and 9(d)). The sensitivity tests suggested that the snow intercept parameter and transfer processes could both have impact on snow production.

The snow contents even with these sensitivity tests are still smaller than the Goddard 3ICE-graupel scheme (Fig. 6(d)). In addition, the level of maximum snow profile is different between sensitivity tests and Thompson microphysical schemes (Fig. 6(a)). Note that the level of the maximum graupel profile is about 500 hPa in all sensitivity tests, and original Purdue Lin, WSM6, Thompson and Goddard 3ICE-graupel scheme).

Additional tests may be required to fully explain the differences between the schemes. For example, a simple method was proposed for the WSM6 scheme (Dudhia *et al.* 2007) to alleviate the problem of species separation by revising the paradigm that a particle must be either graupel or snow, particularly in the treatment of its fall speed, and hence trajectory, thus preventing a false separation due to their relative sedimentation rates. This new improvement could allow for more snow production.

5. Summary

Three different Goddard bulk liquid-ice microphysical schemes were implemented into WRF. They are the 2ICE (cloud ice and snow), 3ICE-graupel (cloud ice, snow and graupel) and 3ICE-hail (cloud ice, snow and hail) schemes. These microphysical schemes also

include warm rain processes with two classes of liquid phase (cloud water and rain). The Goddard bulk schemes allow three different options for saturation adjustments. The Goddard bulk schemes' performance was tested and compared with three other WRF microphysical schemes (i.e., Purdue LIN, WSM6 and Thompson) for a midlatitude convective system and an Atlantic hurricane case. The major highlights are as follows:

- The Goddard 3ICE scheme with a cloud ice-snow-hail configuration led to a better simulation of the summer midlatitude convective line system than the other schemes. The 3ICE-hail scheme also simulated less light precipitation and more moderate rainfall. These results seem to be in better agreement with observations. The optimal mix of cloud ice-snow-hail for midlatitude squall systems was also found in other CRM simulations (Fovell and Ogura 1998; Tao *et al.* 1995, 1996).
- The microphysical schemes do not have a major impact on hurricane track; however, they can affect the MSLP significantly. The simulated hurricanes were consistently stronger than was observed in all of the WRF runs regardless of the microphysical schemes. The simulated hurricane is strongest prior to landfall and starts to weaken after landfall, which is in good agreement with observations.
- The Thompson scheme simulated less light precipitation and more moderate rainfall in good agreement with observations for the IHOP case. Its simulated intensity for Hurricane Katrina is similar to the Goddard 2ICE scheme. However, the Thompson scheme produced very little cloud ice in both the IHOP and hurricane cases. Another characteristic of the Thompson scheme is that the simulated graupel reaches much lower than the other schemes in the IHOP case.

- The Purdue Lin and WSM6 schemes simulated much less snow than the other schemes for both the midlatitude convective system and the hurricane case. The vertical distribution of precipitating particles is quite important for accurate satellite rainfall and latent heating retrieval (Kummerow *et al.* 1996; Lang *et al.* 2007; and Olson *et al.* 2006).
- Sensitivity tests suggested that snow productions could be increased by increasing the snow intercept, turning off the auto-conversion from snow to graupel and reducing the transfer processes from cloud-sized particles to precipitation-sized ice in the Purdue Lin and WSM6 schemes.

The sensitivity of the Goddard microphysical schemes was only tested for two cases, and comparisons with observations only focused on organization (including track and intensity), the vertical distribution of cloud species, and rainfall intensity. More detailed comparisons with observations will be performed in Part II (Shi *et al.* 2007). Additional case studies to address microphysical processes, including more comprehensive microphysical sensitivity testing (e.g., turning off certain conversion processes from one cloud species to another), will be considered in future research.

The newly revised Goddard microphysical schemes were linked with a sophisticated land information system (Kumar *et al.* 2007). Goddard longwave and shortwave radiative transfer processes with explicit, interactive cloud-radiation processes (with optical properties consistent with the simulated microphysical properties) are being implemented into WRF. The performance of the Goddard cloud-radiation physics will be presented in a future paper.

6. Acknowledgements

The authors thank Dr. D. Anderson at NASA headquarters for his support under the Cloud Modeling and Analysis Initiative (CMAI) program. The GCE microphysics development and improvements are mainly supported by the NASA Headquarters Atmospheric Dynamics and Thermodynamics Program and TRMM. The first author and Dr. J. Simpson are grateful to Dr. R. Kakar at NASA headquarters for his support of GCE development over the past decade.

Acknowledgment is also made to the NASA Goddard Space Flight Center and the NASA Ames Research Center for computer time used in this research.

7. References

Chen, F., and J. Dudhia, 2001: Coupling an advanced land-surface / hydrology model with the Penn State / NCAR MM5 modeling system.. Part I: Model description and implementation. *Mon. Wea. Rev.*, **129**, 569-585.

Chen, S.-H., and W.-Y. Sun, 2002: A one-dimensional time dependent cloud model, *J. Meteor. Soc. Japan*, **80**, 99-118.

Chen, S. S., J. F. Price, W. Zhao, M. A. Donelan, and E. J. Walsh, 2007: The CBLAST-Hurricane Program and the next-generation fully coupled atmosphere-wave-ocean models for hurricane research and prediction. *Bull. Amer. Meteor. Soc*, **88**, 311-317.

Chou, M.-D., and M. J. Suarez, 1999: A shortwave radiation Parameterization for atmospheric studies. 15, NASA/TM-104606. pp40.

Colle B. A., and Y. Zeng, 2004b: Bulk microphysical sensitivities and pathways within the MM5 for orographic precipitation. Part II: Impact of different bulk schemes, barrier width, and freezing level. *Mon. Wea. Rev.*, **132**, 2802–2815

Dudhia, J., 1989: Numerical study of convection observed during the winter monsoon experiment using a mesoscale two-dimensional model, *J. Atmos. Sci.*, **46**, 3077-3107.

Dudhia, J., S.-Y. Hong, and K.-S. Lim, 2007: A new method for representing mixed-phase particle fall speeds in bulk microphysics parameterizations. (to be submitted).

Ferrier, B.S., W.-K. Tao and J. Simpson,1995: A double-moment multiple-phase four-class bulk ice scheme. Part II: Simulations of convective storms in different large-scale environments and comparisons with other bulk parameterizations. *J. Atmos Sci.*, **52**, 1001-1033.

Fovell, R. G., and Y. Ogura, 1988: Numerical simulation of a midlatitude squall line in two-dimensions. *J. Atmos. Sci.*, **45**, 3846-3879.

Fritsch, J. M., and R. E. Carbone, 2002: Research and development to improve quantitative precipitation forecasts in the warm season: A synopsis of the March 2002 USWRP Workshop and statement of priority recommendations. *Technical report to UEWRP Science Committee*,134pp.

Fu, Q., S. K. Krueger, and K.-N. Liou, 1995: Interaction of radiation and convection in simulated tropical cloud clusters. *J. Atmos. Sci.*, **52**, 1310-1328.

Grell, G. A., and D. Devenyi, 2002: A generalized approach to parameterizing convection combining ensemble and data assimilation techniques. *Geophy. Res. Lett.*, **29**, Article

1693.

Hong, S.-Y., H.-M. H. Juang, and Q. Zhao, 1998: Implementation of prognostic cloud scheme for a regional spectral model. *Mon. Wea. Rev.*, **126**, 2621-2639.

Hong, S.-Y., J. Dudhia, and S.-H. Chen, 2004: A revised approach to ice microphysical processes for the bulk parameterization of clouds and precipitation, *Mon. Wea., Rev.*, 132, 103-120.

Hong, S.-Y., and J.-O. J. Lim, 2006: The WRF Single-Moment 6-Class Microphysics Scheme (WSM6). *J. Korean Meteor. Soc.*, **42**, 2, 129-151.

Houze, R. A., Jr., S. S. Chen, W.-C. Lee, R. F. Rogers, J. A. Moore, G. J. Stossmeister, M. M. Bell, J. Cetrone, W. Zhao, and S. R. Brodzik, 2006: The hurricane rainband and intensity change experiment, *Bull. Amer. Meteor. Soc.*, **87**, 1503-1521.

Kain, J. S., and J. M. Frirsch, 1990: A one-dimensional entraining/detraining plume model and its application in convective parameterization. *J. Atmos. Sci.*, **47**, 2784-2802.

Kain, J. S., and J. M. Frirsch, 1993: Convective parameterization for mesoscale models: The Kain-Fritsch scheme. The representation of cumulus convection in numerical models. K. A. Emanuel and D. J. Raymond, Eds., *Amer. Meteor. Soc.*, 246 pp.

Krueger, S. K., Q. Fu, K. N. Liou, and H.-N. Chin, 1995: Improvments of an ice-phase microphysics parameterization for use in numerical simulations of tropical convection. *J. Appl. Meteor.*, **34**, 281–287.

Kumar, S. V., C. D. Peters-Lidard, J. E. Eastman, W.-K. Tao, 2006: An integrated high resolution hydrometeorological modeling system using LIS and WRF, *Environmental Modeling & Software,* (submitted).

Kummerow, C., W. S. Olson, and L. Giglio, 1996: A simplified scheme for obtaining precipitation and vertical hydrometeor profiles from passive microwave sensors. IEEE Trans. *Geosci. Remote Sens.*, **34**, 1213–1232.

Lang, S., W.-K. Tao, R. Cifelli, W. Olson, J. Halverson, S. Rutledge, and J. Simpson, 2007: Improving simulations of convective system from TRMM LBA: Easterly and Westerly regimes. *J. Atmos. Sci.*, (**in press**).

Lin, Y.-L., R. D. Farley and H. D. Orville, 1983: Bulk parameterization of the snow field in a cloud model. *J. Clim. Appl. Meteor.*, **22**, 1065-1092.

Liu, Y., D.-L. Zhang, and M. K. Yau, 1997: A multiscale numerical study of Hurricane Andrew (1992)/ Part I: An explicit simulation. *Mon. Wea. Rev.*, **125**, 3073-3093.

Lord, S. J., H. E. Willoughby and J. M. Piotrowicz, 1984: Role of a parameterized ice-phase microphysics in an axisymmetric, non-hydrostatic tropical cyclone model. *J. Atmos. Sci.*, **41**, 2836-2848.

McCumber, M., W.-K. Tao, J. Simpson, R. Penc, and S.-T. Soong, 1991: Comparison of ice-phase microphysical parameterization schemes using numerical simulations of tropical convection. *J. Appl. Meteor.*, **30**, 985-1004.

Mellor, G. L., and T. Yamada, 1992: Development of a turbulence closure model for geophysical fluid problems, Rev. Geophys. Spaxe Phys., 20, 851-875.

Mlawer, E. J., S. J. Taubman, P. D. Brown, M. J. Jacono, and S. A. Clough, 1997: Radiative transfer for inhomogeneous atmosphere: RRTM, a validated correlated-k model for the longwave. *J. Geophys. Res.*, **102**(D14), 16663-16682.

Monin, A. S., and A. M. Obukhov, 1954: Basic laws of turbulent mixing in the surface layer of the atmosphere. *Contrib. Geophys. Inst. Acad. Sci.* USSR, (151), 163-187 (in Russian).

Nicholls, M. E., 1987: A comparison of the results of a two-dimensional numerical simulation of a tropical squall line with observations. *Mon. Wea. Rev.*, **115,** 3055–3077.

Olson, W.-S., C. D. Kummerow,, S. Yang, G. W. Petty, **W.-K. Tao**, T. L. Bell, S. A. Braun, Y. Wang, S. E. Lang, D. E. Johnson and C. Chiu, 2006: Precipitation and latent heating distributions from satellite passive microwave radiometry Part I: Method and uncertainties. *J. Applied Meteor.*, **45**, 702-720.

Reisner, J. R., R. M. Rasmussen, and R. T. Bruintjes, 1998: Explicit forecasting of supercooled liquid water in winter storms using the MM5 mesoscale model. *Quart. J. Roy. Meteor. Soc.*, **124**, 1071-1107.

Rogers, R., M. Black, S. S. Chen, and R. Black, 2007: Evaluating microphysical parameterization schemes for use in hurricane environments. Part I; Comparisons with observations. *J. Atmos. Sci.*, **64**, in press. (Available at http://orca.rsmas.miami.edu/~schen/publications/)

Rutledge, S.A., and P.V. Hobbs, 1984: The mesoscale and microscale structure and organization of clouds and precipitation in mid-latitude clouds. Part XII: A diagnostic modeling study of precipitation development in narrow cold frontal rainbands. *J. Atmos. Sci.*, **41**, 2949-2972.

Soong, S.-T., and Y. Ogura, 1973: A comparison between axisymmetric and slab-symmetric cumulus cloud models. *J. Atmos. Sci.*, **30**, 879-893.

Shi, J., W.-K. Tao, S. Chen, S. Lang, C. Peters-Lidard and J. Simpson, 2007: Revised bulk-microphysical schemes for studying precipitation processes: Part II: Comparison with observations, *Mon. Wea. Rev.*, (to be submitted).

Tao, W.-K., and J. Simpson, 1989: Modeling study of a tropical squall-type convective line.

J. Atmos. Sci., **46**, 177-202.

Tao, W.-K., J. Simpson and M. McCumber, 1989: An ice-water saturation adjustment. *Mon. Wea. Rev.*, **117**, 231-235.

Tao, W.-K., and J. Simpson, 1993: The Goddard Cumulus Ensemble Model. Part I: Model description. *Terrestrial, Atmospheric and Oceanic Sciences,* **4**, 19-54.

Tao, W.-K., J. Scala, B. Ferrier and J. Simpson, 1995: The effects of melting processes on the development of a tropical and a midlatitude squall line, *J. Atmos. Sci.*, **52**, 1934-1948.

Tao, W.-K., J. Simpson, S. Lang, C.-H. Sui, B. Ferrier, and M.-D. Chou, 1996: Mechanisms of cloud-radiation interaction in the Tropics and mid-latitudes. *J. Atmos. Sci* ., **53**, 2624-2651.

Tao, W.-K., J. Simpson, D. Baker, S. Braun, M.-D. Chou, B. Ferrier, D. Johnson, A. Khain, S. Lang, B. Lynn, C.-L. Shie, D. Starr, C.-H. Sui, Y. Wang and P. Wetzel, 2003a: Microphysics, Radiation and Surface Processes in a Non-hydrostatic Model, *Meteorology and Atmospheric Physics,* **82**, 97-137.

Tao, W.-K., C.-L. Shie, D. Johnson, R. Johnson, S. Braun, J. Simpson, and P. E. Ciesielski, 2003b*:* Convective Systems over South China Sea: Cloud-Resolving Model Simulations *J. Atmos. Sci.*, **60**, 2929-2956.

Thompson, G., R. M. Rasmussen, and K. Manning, 2004: Explicit forecasts of winter precipitation using an improved bulk microphysics scheme. Part I: Description and sensitivity analysis, *Mon. Wea., Rev.*, **132**, 519-542.

Thompson, G., P. R. Field, W. D. Hall and R. M. Rasmussen, 2007: A new bulk microphysical parameterization for WRF (&MM5).

Wicker, L. J., and W. C. Skamarock, 2002: Time splitting methods for elastic models using forward time schemes. *Mon. Wea. Rev.*, **130**, 2088-2097. Wu X., W. D. Hall, W. W. Grabowski, M. W. Moncrieff, W. D. Collins, and J. T. Kiehl, 1999: Long-term behavior of cloud systems in TOGA COARE and their interactions with radiative and surface processes. Part II: Effects of ice microphysics on cloud-radiation interaction. *J. Atmos. Sci.*, **56**, 3177–3195

Yuter, S. E., and Houze R. A. Jr., 1995: Three-dimensional kinematic and microphysical evolution of Florida cumulonimbus. Part II: Frequency distributions of vertical velocity, reflectivity, and differential reflectivity. Mon. Wea. Rev., 123, 1941–1963.

Yoshizaki, M., 1986: Numerical simulations of tropical squall-line clusters: Two-dimensional model. *J. Meteor. Soc. Japan,* **64,** 469–491.

Zhang, D.-L., 1989: The effect of parameterized ice microphysics on the simulation of vortex circulation with a mesoscale hydroststic model. *Tellus*, **41A,** 132-147.

Zhu, T., and D.-L. Zhang, 2004: Numerical simulation of Hurricane Bonnie (1998). Part II: Sensitivity to varying cloud microphysical processes. *J. Atmos. Sci.*, **63**, 109-126.

Figure Captions

Fig. 1 **(a)** Observed WSR-88D composite reflectivity at 00Z (top), 03Z (middle), and 06Z (bottom) 13 June 2002 (Source: NOAA/NESDIS Satellite and Information Service). **(b)** The left panel shows the horizontal rain intensity pattern associated with Hurricane Katrina as observed by TRMM. Rain rates in the center of the swath are from the TRMM Precipitation Radar (PR), and those in the outer portion are from the TRMM Microwave Instrument (TMI). The rain rates are overlaid on infrared (IR) data from the TRMM Visible Infrared Scanner (VIRS). The right panel shows a 3D rendering of Hurricane Katrina constructed from TRMM PR data with a cutaway view through the eye of the storm. Tall towers are indicated in red on the isosurface. Images are courtesy of H. Pierce (NASA GSFC/SSAI).

Fig. 2 Nesting configuration used for the IHOP simulations. Horizontal resolutions for domains 1, 2, and 3, are 9, 3 and 1 km, respectively.

Fig. 3 Nesting configuration used for the Hurricane Kartrina simulations. Horizontal resolutions for domains 1, 2 and 3, are 15, 5 and 1.667 km, respectively.

Fig. 4.1 Simulated radar reflectivity (in dBZ) using WRF for six different microphysical schemes: the **(a)** Thomson, **(b)** WSM6 and **(c)** Purdue-Lin scheme are part of WRF's current options and **(d)** 3ICE-graupel, **(e)** 2ICE and **(f)** 3ICE-hail are the Goddard options. These radar reflectivity are calculated based on model simulated

precipitation particles (rain, snow and graupe/hail) at 24-hour model integration time corresponding to 00Z 13 2002 (top panel of Fig. 1(a)).

Fig. 4.2 As Fig. 4.1 except at 27-hour model integration time.

Fig. 4.3 As Fig. 4.1 except at 30-hour model integration time.

Fig. 5 PDF (probability distribution function) of WRF simulated hourly-accumulated rainfall intensity from six different microphysical schemes. The observed PDF derived from hourly MESONET rain gauge data is also shown for comparison.

Fig. 6 Vertical profiles of domain- and 24-hour time-average cloud species (i.e., cloud water, rain, cloud ice, snow and graupel/hail) for the **(a)** Thomson, **(b)** WSM6, **(c)** Purdue-Lin **(d)** 3ICE-graupel, **(e)** 2ICE and **(f)** 3ICE-hail schemes.

Fig. 7 **(a)** Minimum sea level pressure (hPa) obtained from WRF forecasts of Hurricane Katrina using six different microphysical schemes: Thompson, Purdue-Lin, WSM6, 3ICE-graupel, 3ICE-hail and 2ICE from 00Z 27 August to 00Z 30 August 2005. The observed minimum sea level pressure (solid black line) is also shown for comparison. **(b)** shows the corresponding hurricane tracks for the data shown in (a). The best track is shown in black for comparison and was obtained from the National Hurricane Center.

Fig. 8 Same as Fig. 6 except for the Hurricane Katrina case and a 48-hour time-average.

Fig. 9 Vertical profiles of domain- and 24-hour time-average accumulated solid cloud species [cloud ice, snow and graupel]. Black lines represent values from original (non-modified) WSM6 scheme in **(a)** and **(b)** and Purdue-Lin scheme in (c) and (d). Gray lines in (a) are for values from modified WSM6 scheme with WSM6 snow intercept parameter (0.02 cm^{-4}), while in (b) for modified WSM6 scheme with Goddard snow intercept parameter (0.16 cm^{-4}), in (c) for modified Purdue-Lin scheme with Purdue-Lin snow intercept parameter (0.03 cm^{-4}), and in (d) modified Purdue-Lin scheme with Goddard snow intercept parameter (0. 16 cm^{-4}).

Table Captions

Table 1 Domain- and time-average accumulated liquid (warm rain) and solid (ice) water species for the IHOP case. The time-average is based on 24, hourly data outputs.

Table 2 Same as Table 1 except for Hurricane Katrina using 72, hourly data outputs.

	3ICE-Hail	*3ICE-Graupel*	*2Ice*	*WSM6*	*Lin*	*Thompson*
Liquid hydrometeor	**37.3%**	**28.5%**	**15.5%**	**42.5%**	**48.9%**	27.3%
Solid Hydrometeor	**62.7%**	**71.5%**	**84.5%**	**57.5%**	**51.1%**	72.7%

Table 1 Domain- and time-average accumulated liquid (warm rain) and solid (ice) water species for the IHOP case. The time-average is based on 24, hourly data outputs.

	3ICE-Hail	*3ICE-Graupel*	*2Ice*	*WSM6*	*Lin*	*Thompson*
Liquid hydrometeor	**46.6%**	**36.4%**	**24.8%**	**50.4%**	**65.3%**	34.2%
Solid Hydrometeor	**53.4%**	**63.6%**	**75.2%**	**49.6%**	**34.7%**	65.8%

Table 2 Same as Table 1 except for Hurricane Katrina using 72, hourly data outputs

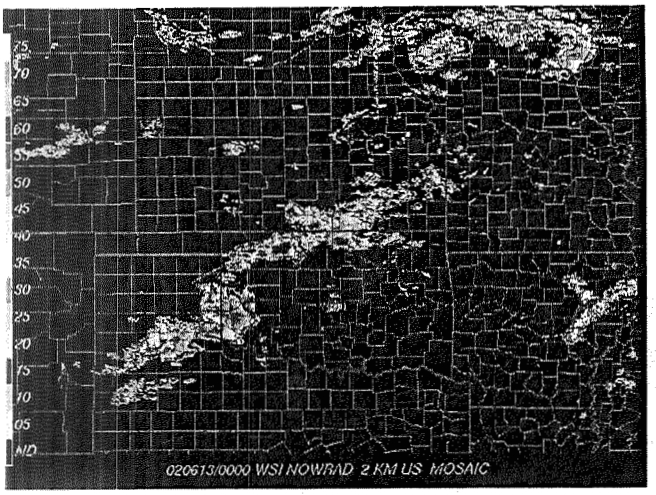

00Z 6/13/2002

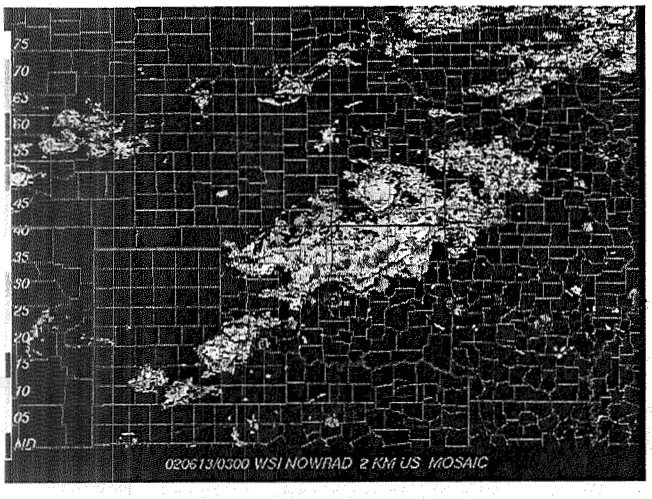

03Z 6/13/2002

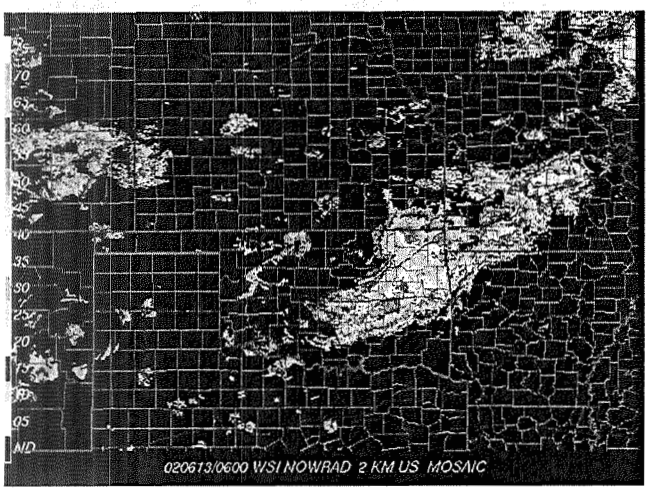

06Z 6/13/2002

Fig. 1(a) Observed WSR-88D composite reflectivity at 00Z 13 (top), 03Z (middle) and 06Z (bottom) June 2002 (Source: NOAA/NESDIS Satellite and Information Service

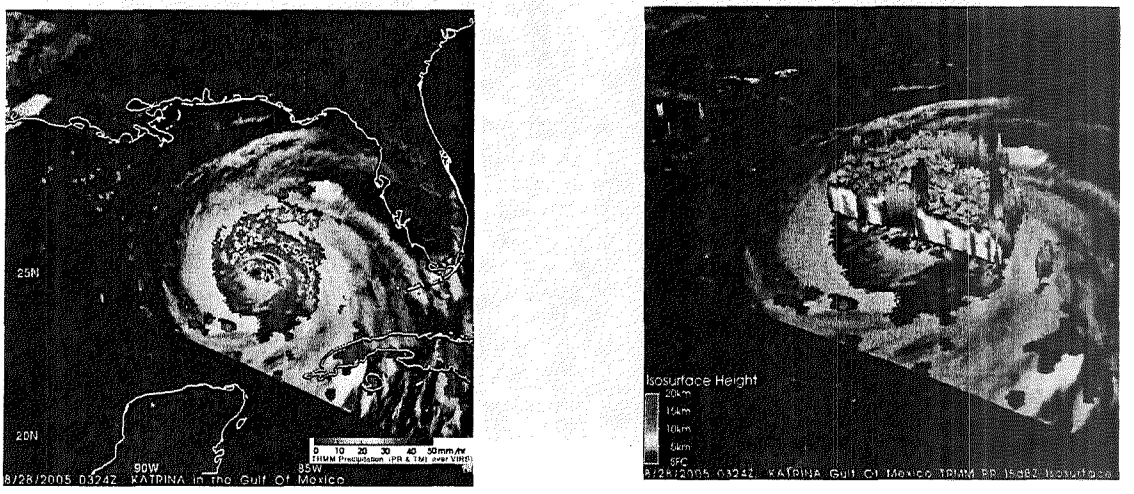

Fig. 1(b) The left panel shows the horizontal rain intensity pattern associated with Hurricane Katrina as observed by TRMM. Rain rates in the center of the swath are from the TRMM Precipitation Radar (PR), and those in the outer portion are from the TRMM Microwave Instrument (TMI). The rain rates are overlaid on infrared (IR) data from the TRMM Visible Infrared Scanner (VIRS). The right panel shows a 3D rendering of Hurricane Katrina constructed from TRMM PR data with a cutaway view through the eye of the storm. Tall towers are indicated in red on the isosurface. Images are courtesy of H. Pierce (NASA GSFC/SSAI).

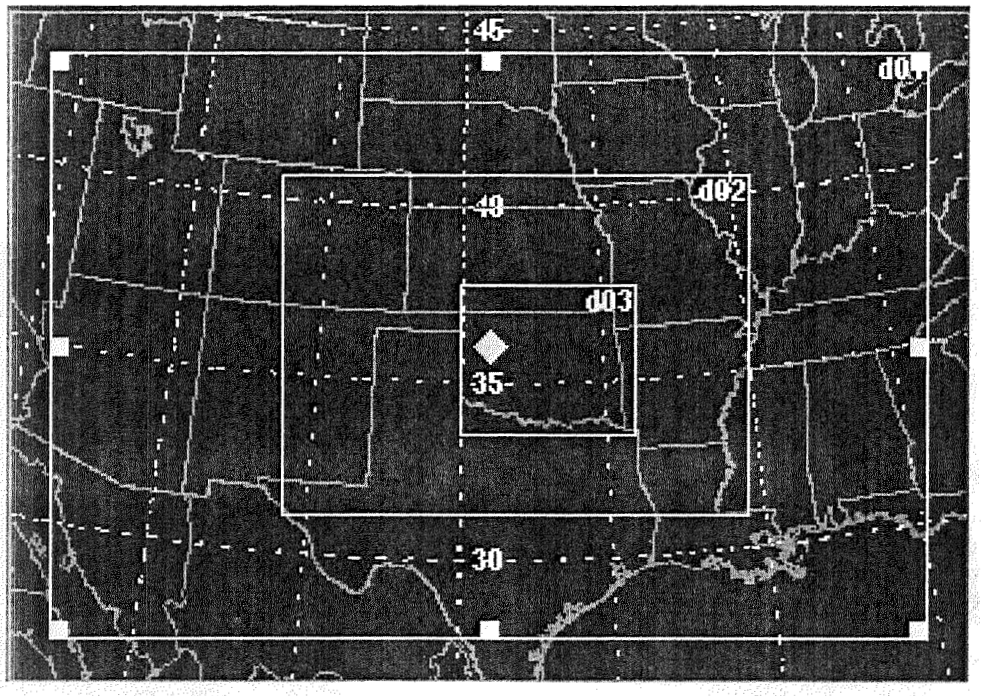

Fig. 2 *Nesting configuration used for the IHOP simulations. Horizontal resolutions for domains 1, 2, and 3, are 9, 3 and 1 km, respectively.*

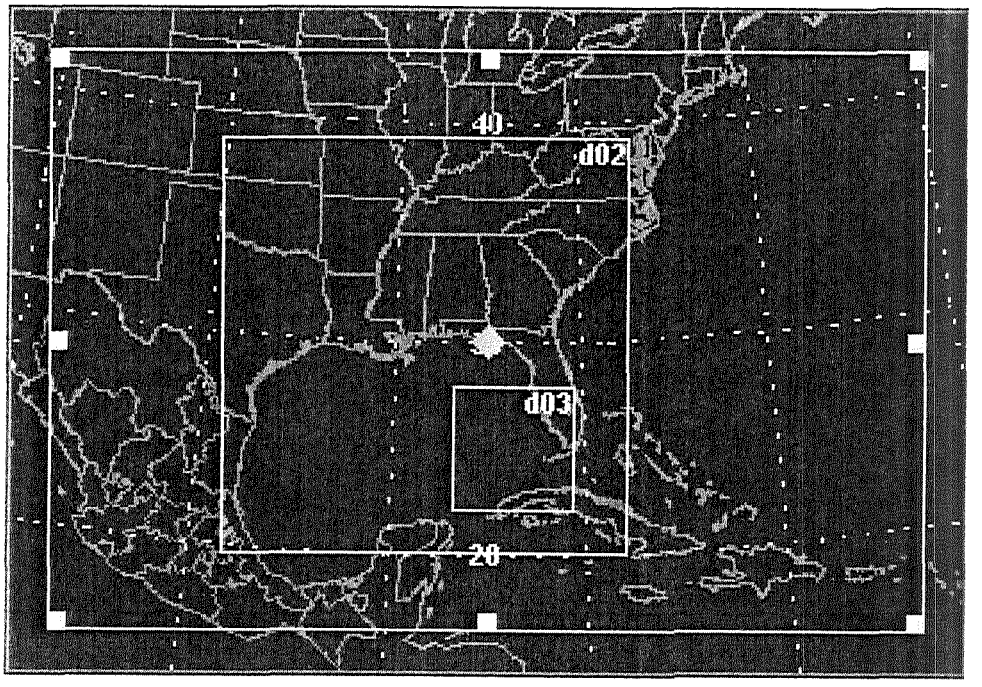

Fig. 3 *Nesting configuration used for the Hurricane Kartrina simulations. Horizontal resolutions for domains 1, 2 and 3, are 15, 5 and 1.667 km, respectively.*

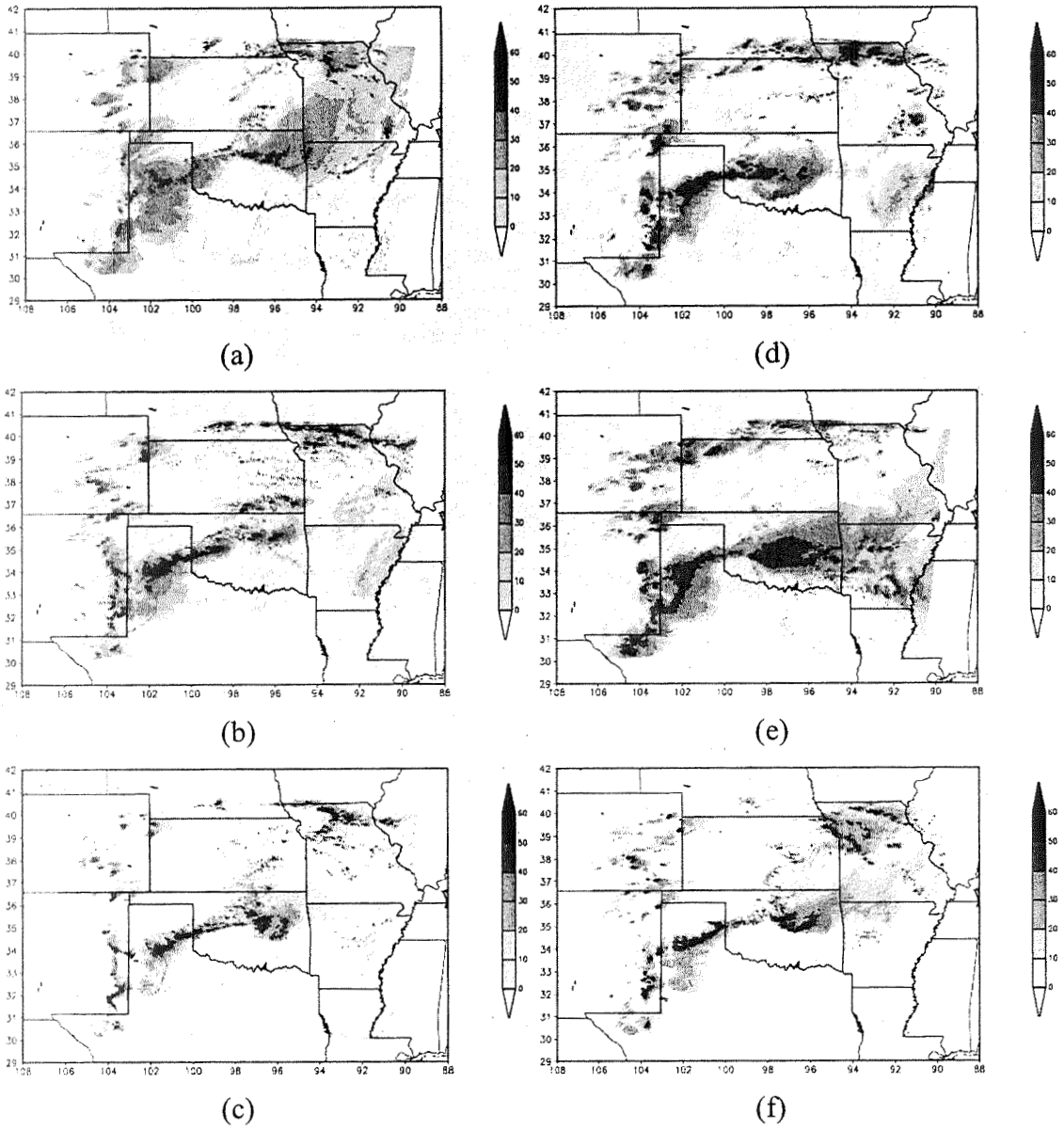

Fig. 4.1 ***Simulated radar reflectivity (in dBZ) using WRF for six different microphysical schemes: the (a) Thomson, (b) WSM6 and (c) Purdue-Lin scheme are part of WRF's current options and (d) 3ICE-graupel, (e) 2ICE and (f) 3ICE-hail are the Goddard options.*** *These radar reflectivity are calculated based on model simulated precipitation particles (rain, snow and graupel/hail) at 24-hour model integration time corresponding to 00Z 13 2002 (top panel of Fig. 1(a)).*

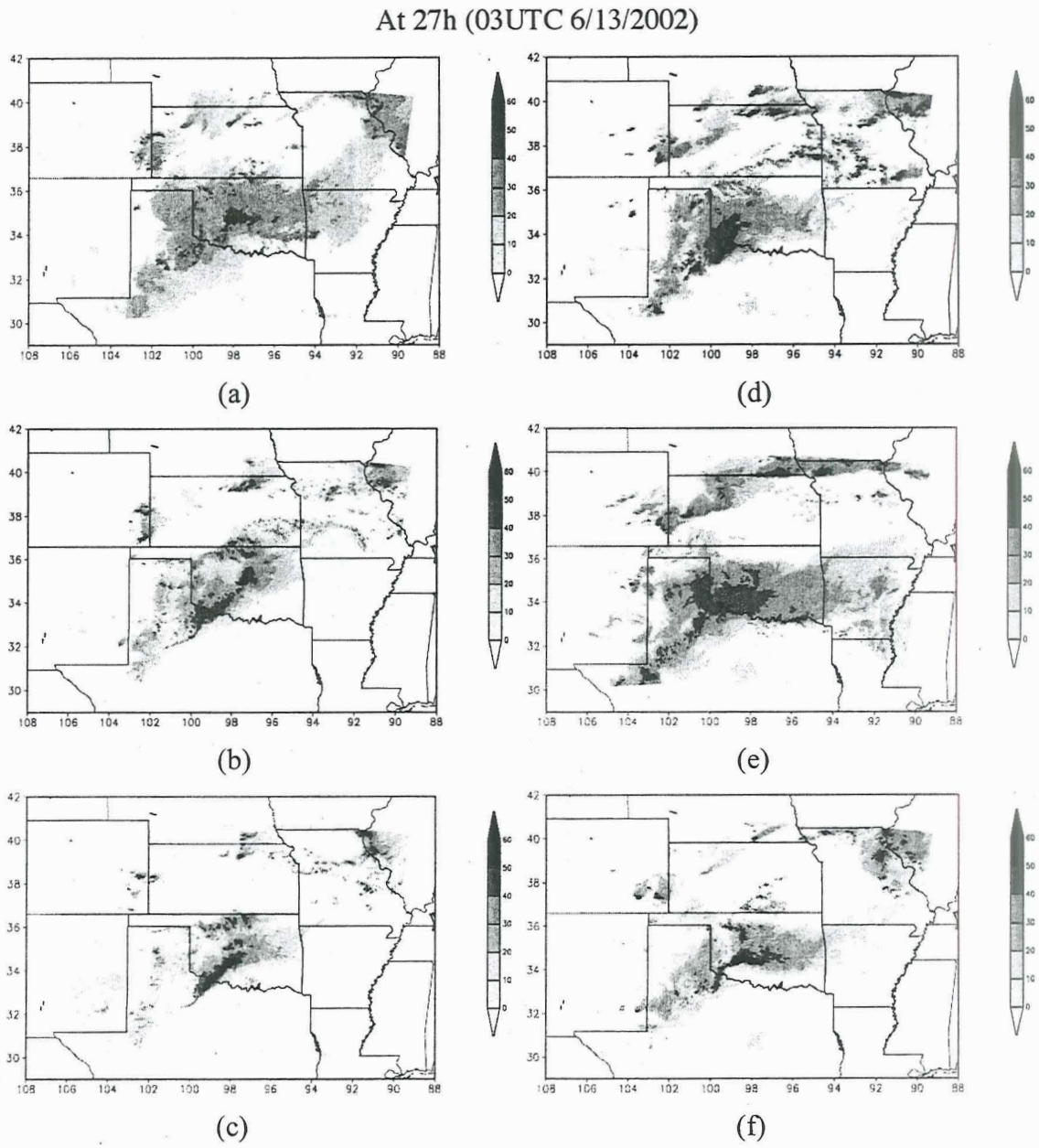

Fig. 4.2 As Fig. 4.1 except at 27-hour model integration time.

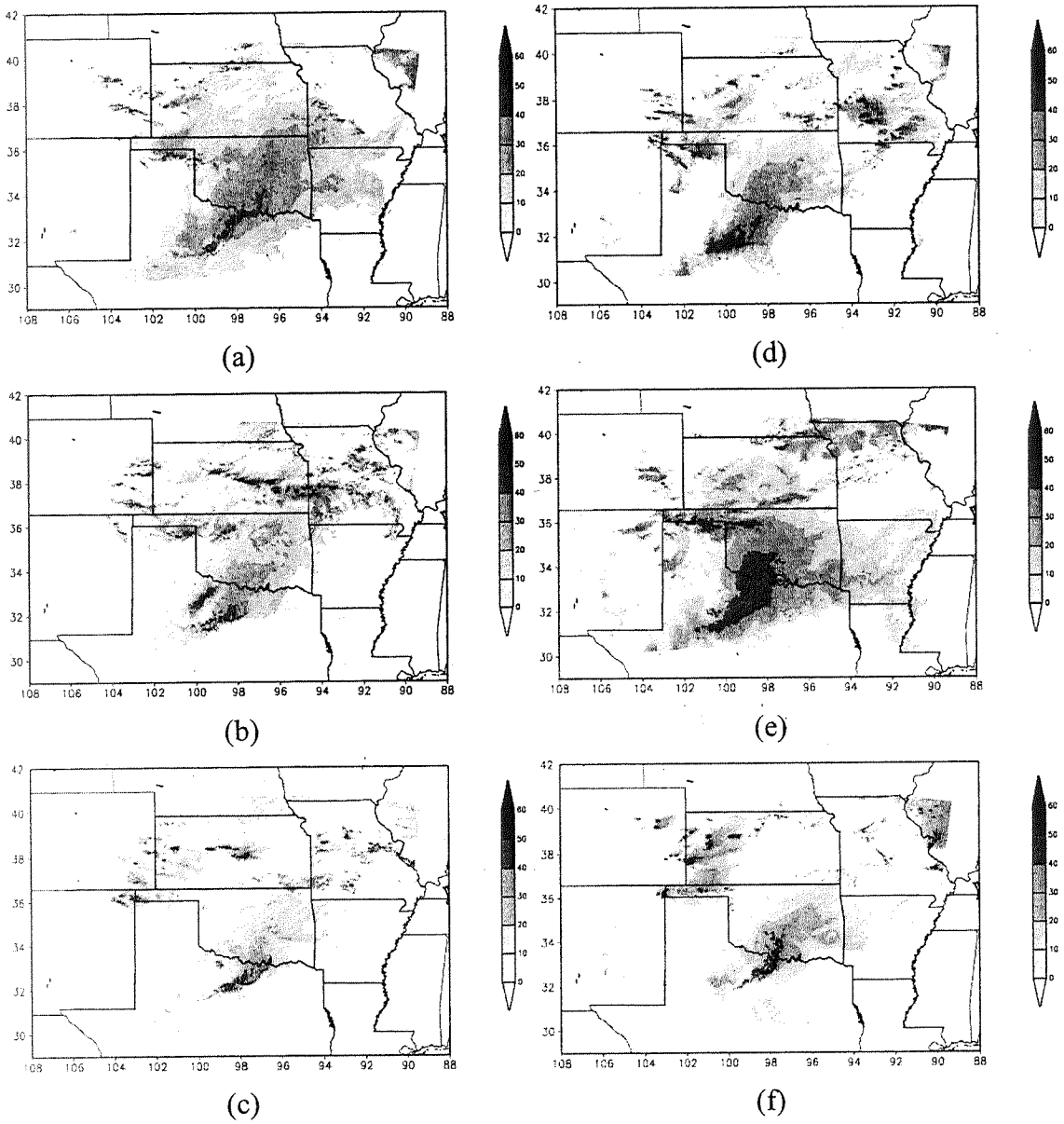

Fig. 4.3 As Fig. 4.2 except at 27-hour model integration time.

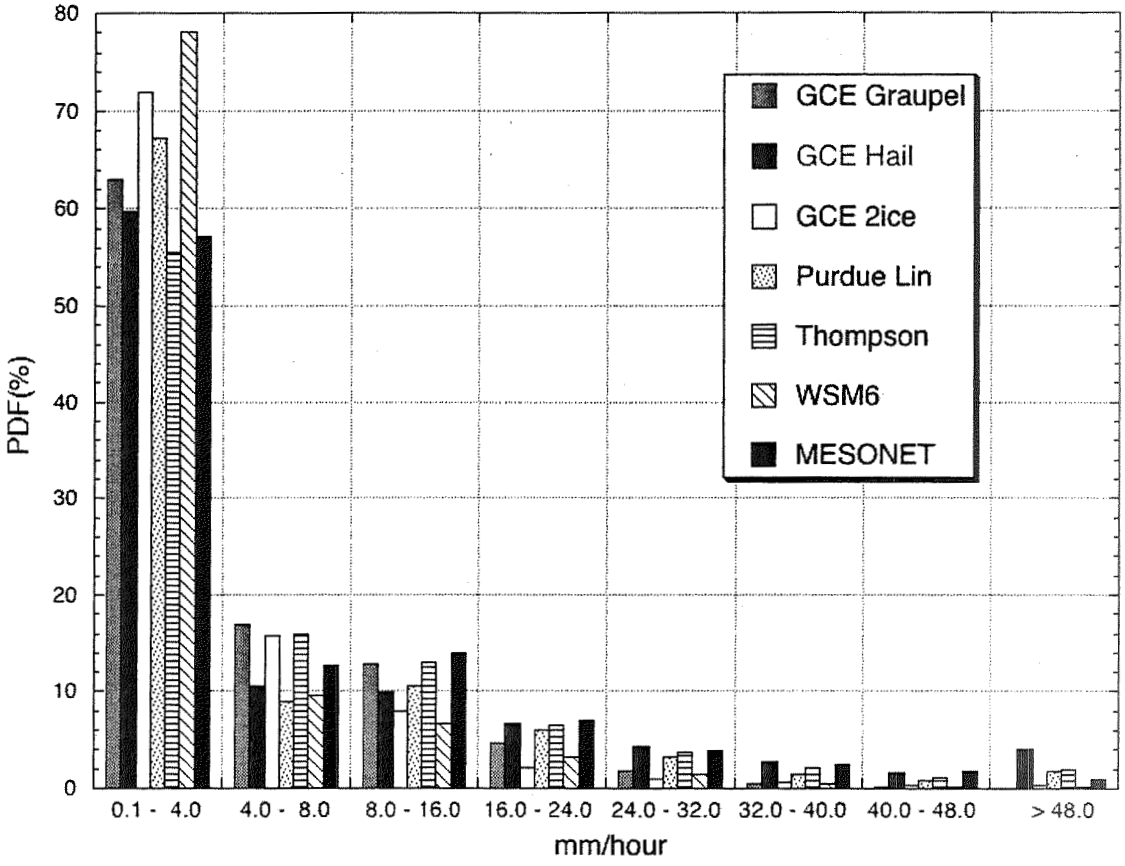

Fig. 5 *PDF (probability distribution function) of WRF simulated hourly-accumulated rainfall intensity from six different microphysical schemes. The observed PDF derived from hourly MESONET rain gauge data is also shown for comparison.*

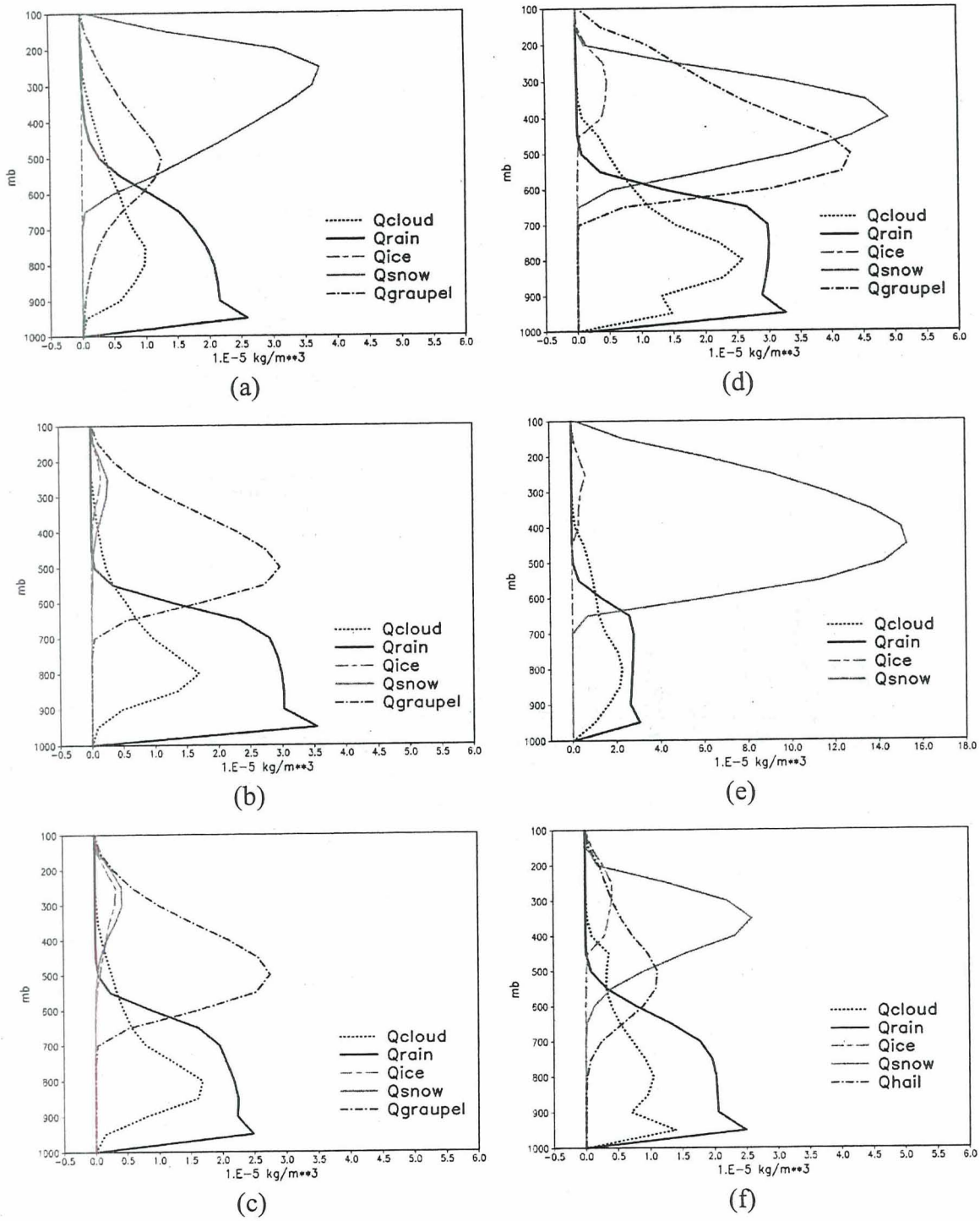

Fig. 6 *Vertical profiles of domain- and 24-hour time-average cloud species (i.e., cloud water, rain, cloud ice, snow and graupel/hail) for the* ***(a)*** *Thomson,* ***(b)*** *WSM6,* ***(c)*** *Purdue-Lin* ***(d)*** *3ICE-graupel,* ***(e)*** *2ICE and* ***(f)*** *3ICE-hail schemes.*

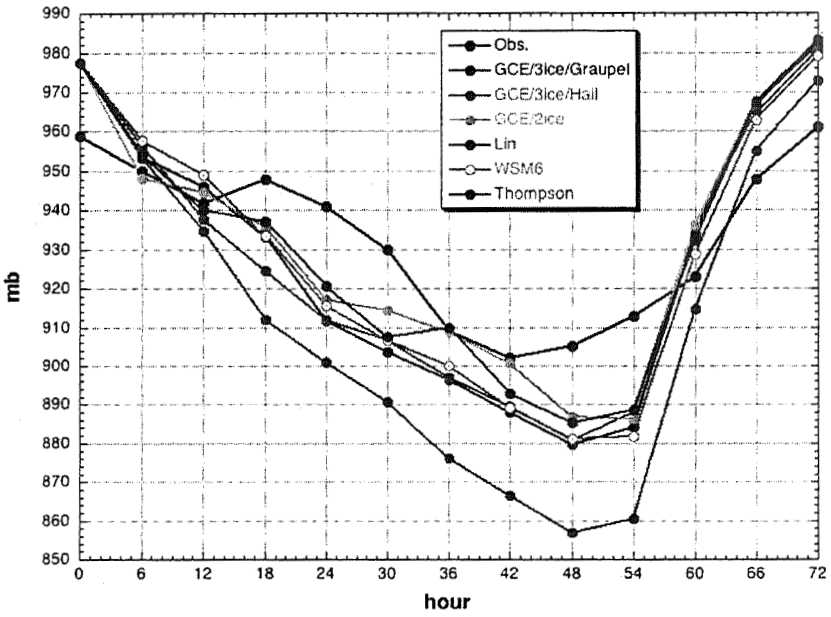

Fig. 7(a) Minimum sea level pressure (hPa) obtained from WRF forecasts of Hurricane Katrina using six different microphysical schemes: Thompson, Purdue-Lin, WSM6, 3ICE-graupel, 3ICE-hail and 2ICE from 00Z 27 August to 00Z 30 August 2005. The observed minimum sea level pressure (solid black line) is also shown for comparison.

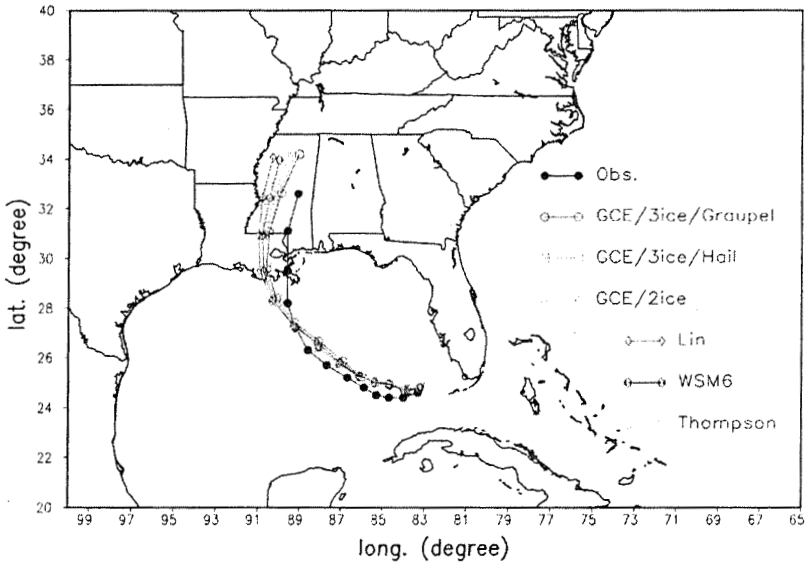

Fig. 7(b) shows the corresponding hurricane tracks for the data shown in (a). The best track is shown in black for comparison and was obtained from the National Hurricane Center.

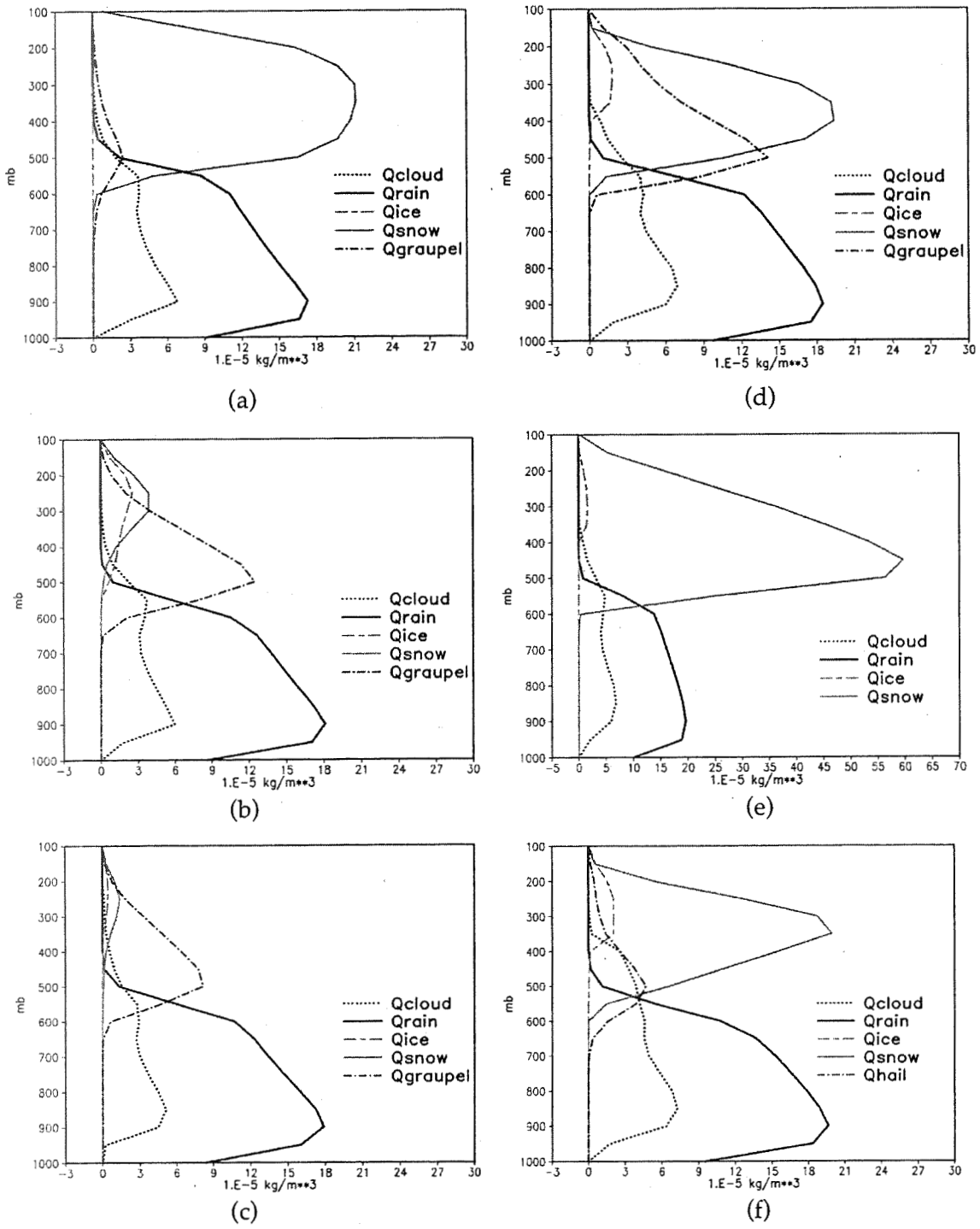

Fig. 8 *Same as Fig. 6 except for the Hurricane Katrina case and a 48-hour time-average.*

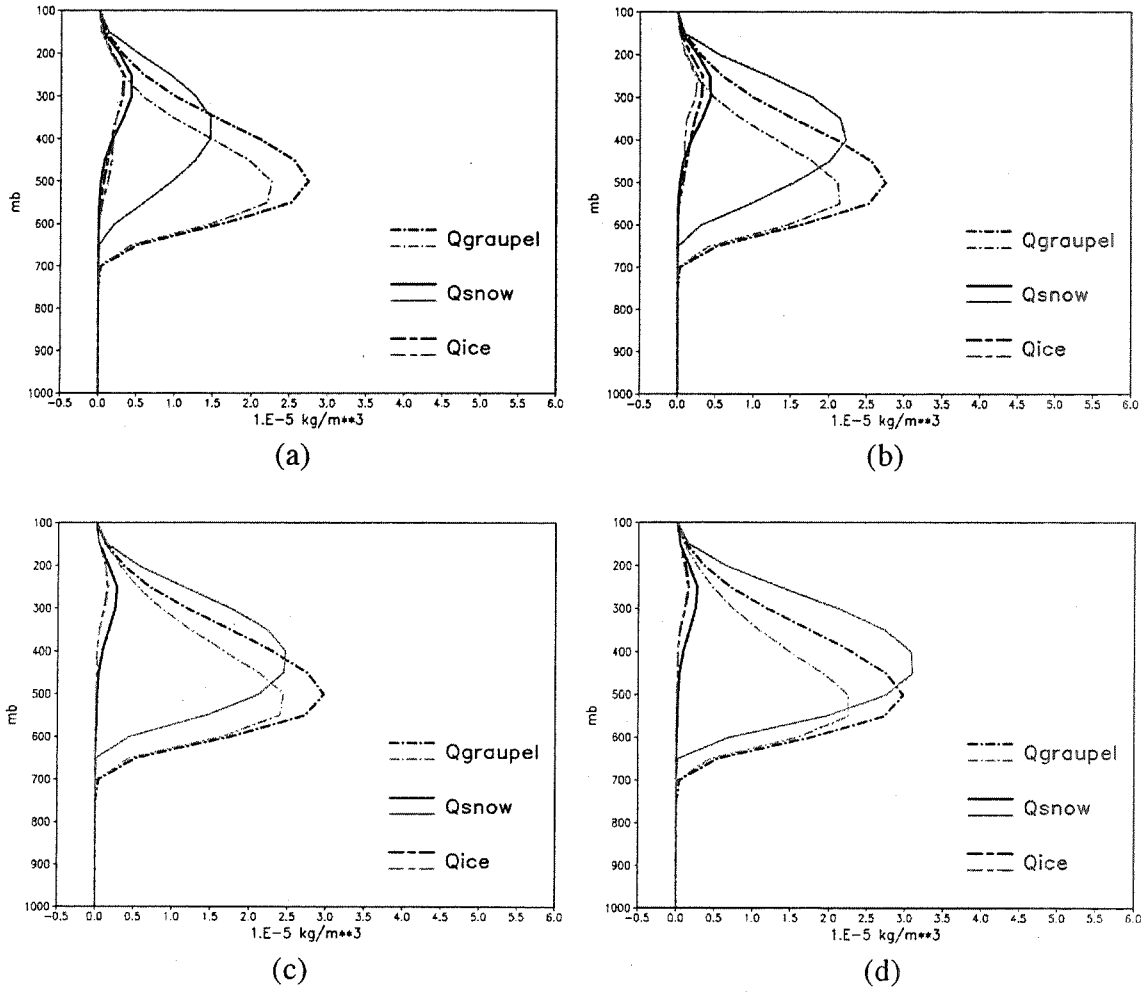

Fig. 9 *Vertical profiles of domain- and 24-hour time-average accumulated solid cloud species [cloud ice, snow and graupel]. Black lines represent values from original (non-modified) WSM6 scheme in* ***(a)*** *and* ***(b)*** *and Purdue-Lin scheme in* ***(c)*** *and* ***(d)****. Gray lines in (a) are for values from modified WSM6 scheme with WSM6 snow intercept parameter (0.02 cm^{-4}), while in (b) for modified WSM6 scheme with Goddard snow intercept parameter (0.16 cm^{-4}), in (c) for modified Purdue-Lin scheme with Purdue-Lin snow intercept parameter (0.03 cm^{-4}), and in (d) modified Purdue-Lin scheme with Goddard snow intercept parameter (0. 16 cm^{-4})*